Label-free electrical quantification of amplified nucleic acids through nanofluidic diodes

Yifan Liu, Levent Yobas *

Department of Electronic and Computer Engineering, The Hong Kong University of Science and Technology, Clear Water Bay, Kowloon, Hong Kong Special Administrative Region

ARTICLE INFO

ABSTRACT

A label-free method of quantifying nucleic acids in polymerase chain reaction (PCR) is described and could be the basis for miniaturized devices that can amplify and detect target nucleic acids in real time. The method takes advantage of ionic current rectification effect discovered in nanofluidic channels exhibiting a broken symmetry in electrochemical potential – nanofluidic diodes. Nanofluidic diodes are prototyped here on nanopipettes readily pulled from individual thin-walled glass capillaries for a proof of concept demonstration yet the basic concept would be applicable to ionic rectifiers constructed through other means. When a nanopipette modified in the tip region with cationic polyelectrolytes is presented with an unpurified PCR product, the tip surface electrostatically interacts with the amplicons and modulates its ionic rectification direction in response to the intrinsic charge of those adsorbed. Modulations are gradual and correlate well with the mass concentration of the amplicons above 2.5 ng/μL, rather than their sizes, with adequate discrimination against the background. Moreover, the tip surface, following a measurement, is regenerated through a layer-by-layer assembly of cationic polyelectrolytes and amplicons. The regenerated tips are capable of measuring distinct mass concentrations without signs of noticeable degradation in sensitivity. Further, the tips are shown capable of reproducing the amplification curve of real-time PCR through sequential steps of surface regeneration and simple electrical readout during the intermediate reaction stages. This suggests that nanopipettes as nanofluidic diodes are at a capacity to be employed for monitoring the PCR progress.

1. Introduction

Nanofluidics – analysis and exploitation of unique phenomena observed in fluids confined to nanoscale structures – has recently attracted burgeoning attention and could potentially lead to advanced devices for chemical and biomedical applications (Eijkel and van den Berg, 2005). For instance, fluidic channels, when scaled down to nanometer regime (typically 1–100 nm), physically confine and stretch nucleic acids (Tegenfeldt et al., 2004). Accordingly, facile integration of nanofluidic components into microfluidics has led to practical systems for entropic sieving of nucleic acids (Han and Craighead, 2000) and high-resolution analysis of stretched DNA molecules (Abad et al., 2011; Kim et al., 2011). Moreover, the unique ion transport behavior through artificial nanochannels has been well studied with a goal to better understand and emulate the function of transmembrane ion channels of biological origin (Cheng and Guo, 2010a; Plecis et al., 2005; Schoch et al., 2008). With a deep insight into its underlying mechanism, the utilization of

this behavior has led to numerous innovative nanoelectrofluidic devices such as nanofluidic field effect transistors (Kalman et al., 2008; Nam et al., 2010, 2009) and ion current diodes for biosensing (Vlassiouk et al., 2009), molecule preconcentration (Hlushkou et al., 2012; Zangle et al., 2010), and molecule delivery (Karnik et al., 2006; Nguyen et al., 2010).

Nanofluidic diodes refer to the nanoporous structures that conduct ion current in one particular direction while suppressing it in the opposite direction (Cheng and Guo, 2010b). Such rectification effect occurs in a nanofluidic channel in which the critical dimension is comparable to the Debye length and ion concentration is governed by the wall surface charge rather than bulk concentration (Karnik et al., 2007; Kovarik et al., 2009; Vlassiouk et al., 2008). The electrical double layers of the walls overlap and the counter-ions dominate the transport. The rectification also requires a broken symmetry across the structure which could be as a result of asymmetric surface charge distribution (Karnik et al., 2007), or lopsided bath concentrations (Cheng and Guo, 2007), or simply asymmetric conical channel profile (Umehara et al., 2006). The effect is explained by the accumulation and depletion of cations and anions at the two entrances of the nanochannel in response to different bias polarities (Cheng and Guo, 2010b).

---

* Corresponding author. Tel.: +852 2358 7068; fax: +852 2358 1485.
  E-mail address: eelyobas@ust.hk (L. Yobas).

A forward bias voltage applied across the nanochannel leads to enrichment of ions and an increased ion conductance whereas a reverse bias voltage depletes ions and results in a decreased ion conductance. Such devices offer new prospects for the controlled separation and sensing of diverse species in aqueous solutions (Ali et al., 2009).

A wealth of biosensing strategies has been reported using nanofluidic channels towards a rapid and cost-effective detection of analytes (Howorka and Siwy, 2009; Piruska et al., 2010). Many, however, apply a resistive-pulse sensing technique, the Coulter-counting principle, as elaborated in the detection of DNA labeled with a nanoparticle translocating through a nanopipette tip (Karhanek et al., 2005). With the recent studies geared towards ion current rectification and the dominant role of surface charge through such structures (Siwy et al., 2004; Siwy, 2006), new sensing strategies exploiting the rectification effect begin to emerge targeting, among various species, metal ions (Sa et al., 2010) and proteins (Ali et al., 2010b; Umehara et al., 2009; Vlassiouk et al., 2009). Moreover, a sequence-specific recognition of nucleic acids has been reported based on the hybridization of a target sequence of single-strand DNA to a complementary probe sequence immobilized on nanofluidic diodes (Ali et al., 2010a; Fu et al., 2009). In those approaches, however, recovery of the sensor surface for repeated measurements appears to be problematic and requires a careful dissociation of the capture probes from the hybridized targets, which poses a great challenge (Fan et al., 2003).

Nanofluidic diodes have not yet been fully explored for the quantitative DNA analysis. In molecular biology, routine DNA analysis often entails polymerase chain reaction (PCR), whereby a few copies of a specific sequence of DNA can be amplified to many copies so as to exceed the limit of detection in the subsequent steps (e.g. capillary or gel electrophoresis). Quantitative or real-time PCR (qPCR) measures the quantity of DNA as it gets amplified, through fluorescent intercalating dyes or sequence-specific reporter probes (Heid et al., 1996). However, the inhibitory effects of such fluorescent reagents and difficulty in miniaturizing and integrating optical components into a portable system for point-of-care diagnosis have elicited a growing interest in detecting PCR products through non-optical means. For instance, electronic field-effect (Fritz et al., 2002; Hou et al., 2006) and electrochemical (Luo and Hsing, 2009) methods have been successfully demonstrated for PCR quantification. Yet a simple, robust and cost-effective label-free strategy is still a remaining challenge. This challenge could potentially be overcome by nanofluidic diodes given their simplistic configuration and label-free real-time electrical readout capability.

In this study, we describe a simple and quantitative method of DNA detection using nanofluidic diodes and, for the first time, demonstrate their capability to quantify PCR products from an unpurified PCR mixture. Nanofluidic diodes used herein, glass nanopipettes, exhibit an asymmetric ion conductance owing to their conical channel (tip) structure and negatively charged surface (Wei et al., 1997). Prepared conveniently from a glass capillary on a commercial bench-top puller, nanopipettes offer a cost-effective route to nanofluidic diodes without the requirement of high-precision sophisticated semiconductor fabrication process. The surface functionalization adopted here draws its principle from electrostatic interactions between the charged polyelectrolyte layers and the device surface as previously implemented on the field-effect DNA sensors (Fritz et al., 2002; Hou et al., 2006). Thus, the tip region of a glass nanopipette gets deposited with a thin layer of an oppositely charged polyelectrolyte, poly-L-lysine (PLL). The charged polyelectrolytes have been recently explored to control the surface potential of quartz nanopipettes and the solid-state conical nanopores (Umehara et al., 2006). However, such nanofluidic diodes functionalized with cationic polyelectrolytes have never been applied before to detect DNA or PCR products but

biotin–streptavidin and antibody–antigen interactions (Umehara et al., 2009). PCR products are double-stranded DNA and their electrostatic association to the tip surface through cationic poly-electrolytes is of particular interest for the convenience of evading the procedures to generate single-stranded sequences which would have been inevitable if hybridization capture probes were used.

The concept is briefly described in Fig. 1. First, a thin layer of PLL is electrostatically adsorbed onto the tip surface to overcompensate the negative surface charge of the native glass in preparation for the electrostatic adsorption of the intrinsically negatively charged DNA. The positive surface charge causes anions to predominantly fill the overlapped double layers and switches permselectivity from cations to anions, reversing the rectification direction of the current–voltage (I–V) relation (Fig. 1A). The rectification direction upon electrostatic adsorption of DNA to the PLL layer reverts back again with perms-electivity in the overlapped double layer having switched back to cations (Fig. 1B). We show that not only does the reversal of the rectification direction signal the presence of DNA but also determine its concentration. This is because the reversal of the rectification direction occurs gradually and at a rate commensurate with DNA mass concentration in the range relevant to PCR conditions. We also show that nanopipettes can be reproducibly used without degradation to their sensitivity upon regenerating their surface with a PLL coating following each measurement. By applying the method to the amplification of a 600-bp segment of human ABO blood group gene, we further demonstrate that nanopipettes allow the PCR progress monitored through simple electrical measurements.

2. Material and methods

2.1. Glass nanopipette fabrication

Glass nanopipettes were fashioned from thin-walled borosilicate glass capillaries with an outer diameter of 1.0 mm and an
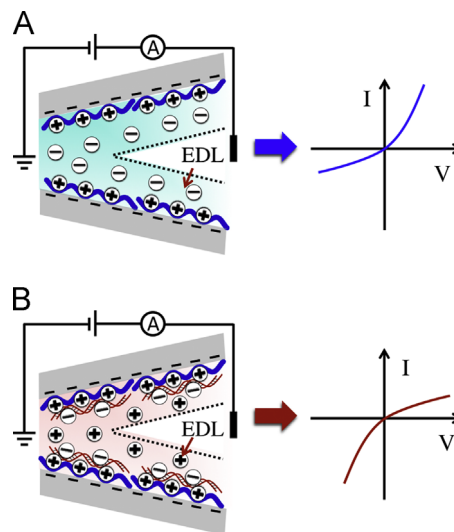
Fig. 1. Biosensor principle. Electrical detection of DNA based on its intrinsic charge modulating the ion current rectification of a nanofluidic diode. Cross-sectional schematics describe a conical nanofluidic diode profile, the nanopipette tip, with the electrical double layers (EDL) overlapped and filled predominantly with the counterions biased under the potentials applied to the electrodes. The current–voltage (I–V) plots are measured to evaluate the relevant ion current rectification. (A) The bare nanopipette tip exposed to cationic polyelectrolyte poly-L-lysine (PLL) adsorbs a thin layer of PLL (blue) on the negatively charged glass surface and thus switches permselectivity to anions; negative currents become suppressed. (B) Subsequently, the same tip exposed to DNA adsorbs a thin layer of DNA (red) on the PLL and accordingly switches permselectivity to cations; positive currents become suppressed. (For interpretation of the references to color in this figure legend, the reader is referred to the web version of this article.)
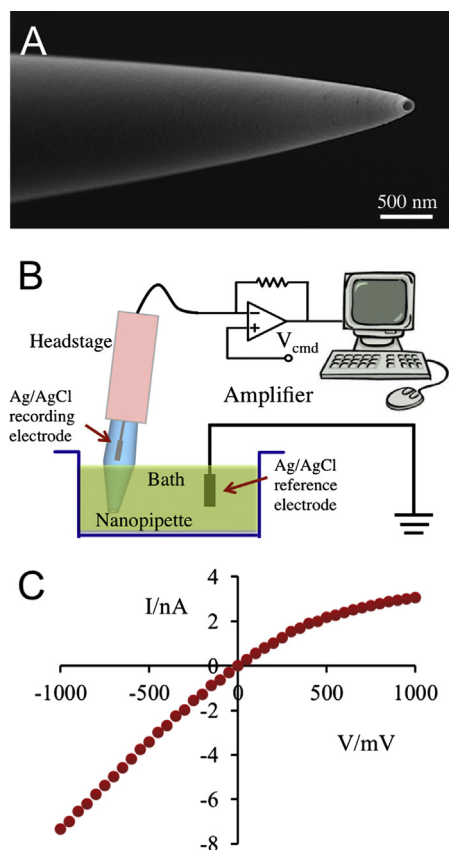
Fig. 2. (A) Scanning electron micrograph of a representative glass nanopipette prepared with the optimized settings here, revealing the inner diameter of a typical tip opening ~80 nm. (B) Schematic representation of the measurement setup. Both the nanopipette and the bath chamber are filled with the PCR buffer. The nanopipette is mounted on the headstage unit of a commercial patch-clamp amplifier for the electrical readout. (C) Representative I–V curve of bare glass nanopipette with the nonlinear characteristic of significantly suppressed positive currents and relatively large negative currents.

inner diameter of 0.75 mm (TW100F-3; World Precision Instrument, Inc.) using a Brown–Flaming micropipette puller (P-97; Sutter Instrument Co.). To obtain nanopipettes with a tip opening below 100 nm, the puller was set to the optimized parameters (Pull=300, Heat=315, Pull=150, Velocity=100, Time=200).

2.2. Polymerase chain reaction

A 600-base-pair (bp) DNA fragment at the O allele of human ABO blood group gene was PCR amplified using a 23-bp forward primer, 5′-TCCCACAGGTCCAATGTTGAGGG-3′, and a 21-bp reverse primer, 5′-CCATCCCTGGGTGAGACGCAG-3′. The PCR buffer consisted of 10 mM Tris–HCl (pH 8.5), 20 mM KCl, 1.5 mM MgCl$_2$ and 1.5 mM (NH$_4$)$_2$SO$_4$. The reaction mixture included $1 \times$ PCR buffer, 30 ng/mL DNA template, 0.2 μM each of forward and reverse primers, 0.2 mM each of dNTPs and 0.05 U/μL Taq polymerase (Qiagen) and went through temperature cycles in GeneAmp PCR System 9700 (Applied Biosystems). Quantitative PCR was performed with Quantitect SYBR Green PCR Kit (Qiagen) at identical template and primers concentration on ABI7300 real-time PCR system (Applied Biosystems). Both the end-point and quantitative PCR implemented a temperature sequence with a 3-min hold at 94 °C, followed by 5–35 cycles of 30 s at 94 °C, 30 s at 50 °C, and 60 s at 72 °C. The reaction mixtures were subsequently kept at 4 °C for measurements or processed with a PCR purification kit (Qiagen) to isolate DNA amplicons.

2.3. Measurement setup

Measurements for each set of I–V curves began with a freshly pulled glass nanopipette backfilled with PCR buffer, inserted with an Ag/AgCl wire (working electrode) and mounted on a headstage unit of a patch-clamp amplifier (EPC 10 USB, HEKA). During measurements, the tip of the nanopipette was kept in PCR buffer at the same composition as the nanopipette fill and presented with an Ag/AgCl wire (reference electrode) connected to the headstage ground. A sequence of voltage pulses (from −1 V to +1 V at an increment of 50 mV and 10 ms each) was applied through the recording Ag/AgCl electrode while the resultant current was recorded on a computer using the software Patchmaster (HEKA). Measurements were taken inside a faraday cage to shield against any electromagnetic interference.

2.4. DNA quantification experiments

DNA ladder (Qiagen) was diluted in PCR buffer at various concentrations from 1 to 80 ng/μL. Surface regeneration of the nanopipette tips was realized by placing the tips first in an aqueous solution of 0.5 mg/mL poly-L-lysine (PLL) hydro-bromide (MW 30,000–70,000; Sigma) for 2 min and then in PCR buffer for 2–5 min to remove unbound species. The tips were also pressurized from a syringe to induce streams for an effective wash in PCR buffer. Reference I–V curves were then collected from the regenerated tips. For the subsequent measurements of analytes, the tips modified with PLL were immersed in a solution of target analyte for 5 min, a duration which is sufficient for electrostatic interactions, and then a wash step in PCR buffer for 5 min before measuring the steady-state I–V curves. Extending the incubation period with the analyte (e.g. 10 min) did not result in a noticeable change in the curves whereas the curves obtained with a shorter incubation time (e.g. 2 min) exhibited reduced repeatability and less deviation from the reference curves. The wash step in PCR buffer was necessary to remove the primers as well as dNTPs, which contribute four negative charges per molecule, and to reduce their background interference in the measurements.

3. Results and discussion

Fig. 2A depicts a scanning electron micrograph of a representative nanopipette prepared with the optimized settings here and reveals the inner diameter of a typical tip opening as ~80 nm. Such tip size is sufficiently small and could lead to a preferential flow of ions under the bias voltages of an opposite polarity and the ionic strengths below 100 mM (Umehara et al., 2009). Accordingly, the bare glass nanopipettes filled with the stated ionic composition of the PCR buffer and with their tips immersed in the same composition (Fig. 2B) exhibit a reasonable rectification response (Fig. 2C). The nonlinear I–V curve displays a characteristic pattern of significantly suppressed positive currents and relatively large negative currents that signify the cations freely moving into the nanopipettes towards the negatively charged electrode. Note that the specific direction of the rectification depends on the surface charge and at the stated pH of the PCR buffer the glass surface of nanopipettes contains silanol groups that are negatively ionized. To quantify the extent of the rectification, we define the ratio $R = \log_2(I_{+1\,V}/I_{-1\,V})$, where $I_{+1\,V}$ and $I_{-1\,V}$ each respectively refers to the positive and negative current level at a fixed bias voltage of +1 V and −1 V. This definition aligns with the definition of rectification previously given for the nanopipette diodes (Umehara et al., 2006). Through a logarithmic function, the reversal of the rectification direction is mapped to the reversal of
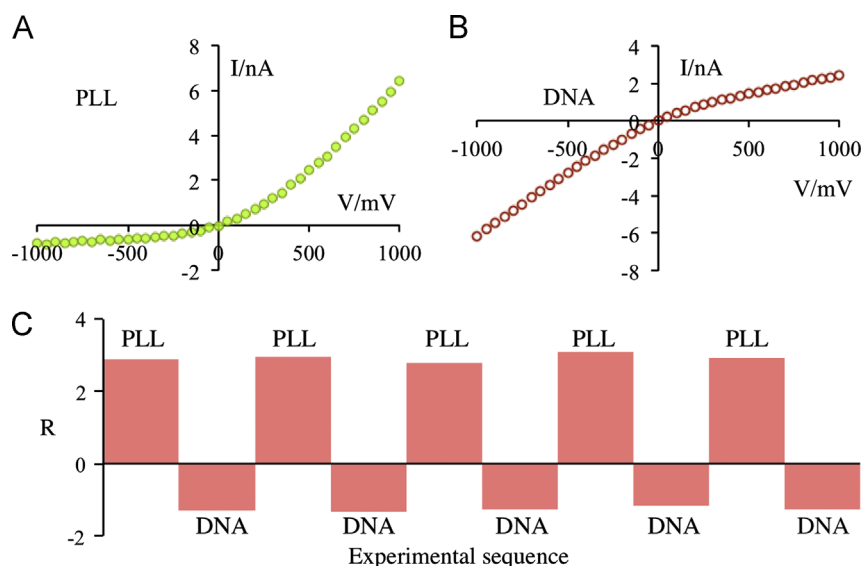
Fig. 3. Reversal of the direction of ion current rectification caused by the surface charge polarity switch with the layer-by-layer assembly of PLL and DNA near the nanopipette tip. (A) and (B) Representative I–V curves of a fresh glass nanopipette tip measured upon (A) a brief exposure to PLL solution and (B) a subsequent exposure to 40 ng/µL DNA ladder. (C) A cyclic pattern of repeatable R values obtained from the same sensor tip subjected to the consecutive cycles of alternating PLL and DNA.

the rectification polarity. The bare glass nanopipettes, based on the measured I–V curves, project a ratio of -0.97 ± 0.17 ($n = 20$).

The nanopipette tip here behaves like a field-effect biosensor; the current rectification, both the degree and the polarity, is a function of the surface charge density and thus influenced by the presence of highly charged biomolecules attached to the surface. To induce electrostatic attraction between the tip and DNA, both being negatively charged, the tip is first deposited with a cationic polyelectrolyte (PLL) to impart a net positive charge. The reversal of the surface charge polarity leads to the reversal of the rectification direction, i.e. $R > 0$ (3.09 ± 0.24 for $n = 20$). This is shown in a representative I–V curve obtained with a PLL-modified tip in Fig. 3A. Exposing the same tip to DNA (40 ng/µL ladder ds-DNA) causes the I–V characteristic to recover its original form as with the bare tip, i.e. $R < 0$, (Fig. 3B). This implies that not only does the attached layer of DNA effectively shield the PLL layer underneath but also leaves a net surface charge density that is negative and thus allows for a fresh layer of PLL to be subsequently deposited. This is important because the same sensor tip can be repeatedly applied across unknown concentrations without the measurements being susceptible to intrinsic variations across separate sensor tips. Moreover, with the same sensor tip having exposed to the consecutive rounds of alternating PLL and DNA, a cyclic pattern of repeatable R values emerges (only five rounds shown in Fig. 3C). This suggests that the diode responds to the net surface charge but not to the overall thickness of the multilayers; the latter is known to increase with the alternating deposition of oppositely charged polyelectrolytes (Decher, 1997). Similar behavior is also noted for field-effect sensors in response to the layer-by-layer assembly of polyelectrolytes on their negatively charged surfaces (Hou et al., 2006). Unlike the field-effect sensors, however, the tip surface here is not the active site to which the top overcompensated surface charge layer must exert its influence on by effectively propagating through the increased multilayer thickness. A clear benefit of our configuration is that the active site, the tip lumen, always remains exposed to the newly adsorbed layer of DNA on the PLL-regenerated surface. Meanwhile, the non-degrading nature of R values here with the number of layers, although it alludes to the surface charge overcompensation observed with the similar constructs on planar surfaces (Zhang et al., 2005), is somewhat in contrast with the recent account of conical nanopores (Ali et al., 2010c). In conical nanopores, the

surface charge of the polyelectrolyte assemblies reportedly shows a dramatic decrease with the increased layers. This is attributed to the nanoconfinement-induced structural reorganization of poly-electrolyte layers on conical nanopores and the lack of which here is probably due to the relatively large size of the tip openings (~80 nm).

To evaluate whether the rectification level correlates with the DNA mass concentration, we obtained I–V plots from five individual nanopipettes prepared under the same conditions. The tips with PLL were exposed to the DNA ladder (50–500 bp) at various dilutions covering the range representative of PCR yield (1–80 ng/µL). The dilutions were applied to the tips consecutively and in no specific order, each following a surface regeneration cycle using PLL. Fig. 4A shares the I–V plots obtained from a single nanopippette. As can be seen, with the increased DNA mass concentration, the rectification gradually reverses its direction from negative to positive current. To better visualize the trend, a dose–response curve was derived based on the absolute shift in rectification, defined here as $\Delta R = |R_{PLL} - R_{DNA}|$, where the ratios R_{PLL} and R_{DNA} correspond to those before and after a nanopipette tip being exposed to a specific mass concentration of DNA, respectively. The shift appears dramatic from 5 to 40 ng/µL for all the nanopipettes suggesting that they could be applied to quantitate a typical PCR yield (Fig. 4B). Nevertheless, also present in a PCR mixture, along with nucleic acids (amplicons, primers, and templates), are dNTPs and Taq polymerase. It is equally important that nanopipette diode be able to stay indifferent to those interfering components while responding to the nucleic acids alone. To assess the level of interference that may arise from such components, we individually tested them on nanopipettes ($n = 5$) at concentrations relevant to PCR and similarly obtained absolute shifts in their corresponding R values (Fig. 5). While the shift caused by Taq polymerase appears faint $\Delta R \sim 0.15$ (not displayed), those by primers and dNTPs are slightly higher, $\Delta R \sim 0.72$ and $\Delta R \sim 0.75$, respectively. However, a far more dramatic change, $\Delta R \sim 4.4$, is registered with the purified product inclusive of amplicons and templates at the conclusion of a 35-cycle PCR. These results suggest that the amplicons have a greater electrostatic association to the PLL layer and as such should dominate the diode response at PCR saturation.

Nanopipette diode is sensitive to the mass concentration of DNA rather than to its size. The rectification shift in response to the forward (23-bp) and reverse (21-bp) primers, 0.2 µM each, at a
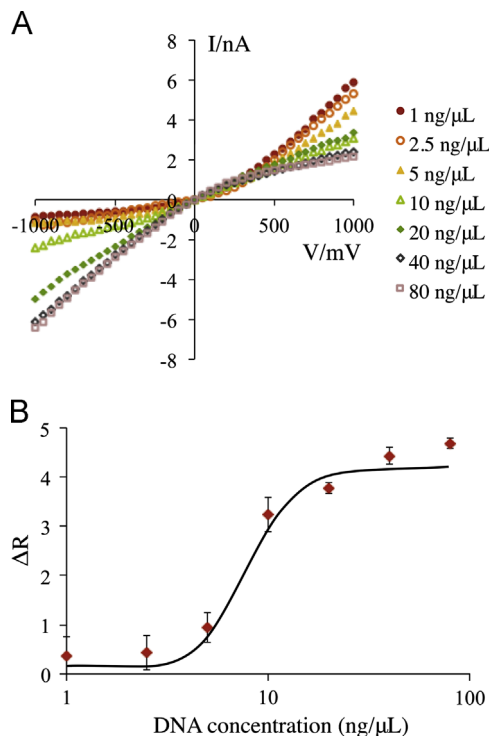
Fig. 4. Biosensor calibration for the quantitative DNA analysis. (A) A set of I–V curves all obtained from a single nanopipette upon the tip exposed to the DNA ladder (50–500 bp) at a specific mass concentration from 1 to 80 ng/μL (the legend). The dilutions were applied to the tip sequentially in no specific order and with each subsequent to a PLL cycle of tip surface regeneration. (B) Dose–response relation derived from the measured I–V curves based on the absolute value of the shift in rectification ratio specific to the mass concentration of DNA. The symbols and error bars refer to the mean and ±1 standard deviation of the values from separate nanopipettes ($n = 5$).
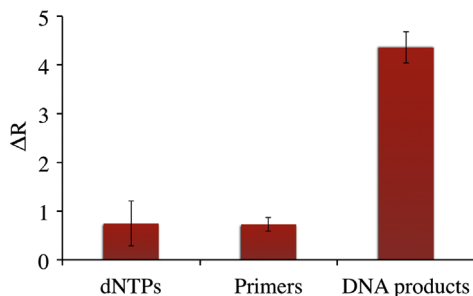

Fig. 5. Biosensor response to the individual components of a PCR mixture: dNTPs (0.2 mM each), forward and reverse primers (0.2 μM each) and a purified 35-cycle PCR product. Each response is expressed in terms of the absolute value of the shift in rectification ratio. The symbols and error bars refer to the mean and ±1 standard deviation of the values from separate nanopipettes ($n = 5$).

mass concentration of ~2.5 ng/μL agrees well with that of DNA ladder (50–500 bp) at the same mass concentration. Similarly, the response to the purified product of 35-cylce PCR (600 bp) at a mass concentration of 45 ng/μL concurs with that to DNA ladder at a concentration of 40 ng/μL. Encouraged by these findings, we utilized the PLL-functionalized nanopipette diodes to measure the products of PCR in which a 600-bp segment of human ABO blood group gene was amplified for various cycles. Fig. 6A shows a set of I–V plots obtained from a representative nanopipette revealing a trend comparable to that observed with the measurements of DNA-ladder at various mass concentrations. Likewise, the rectification, with the increased number of PCR cycles, slowly reverses its direction from negative to positive current. This trend also

shows up in the plot of rectification shift as a function of the number of cycles, which is directly overlaid on the amplification curve from real-time PCR with an intercalating dye (Fig. 6B). Both the electrical and optical readouts show a reasonably good agreement over the linear and plateau phases. A marked increase starts to occur around cycle 10 and reaches saturation by cycle 25. Slightly larger nanopipette readouts in the exponential phase could be attributed to the background interference from dNTPs and primers. The interference caused by these molecules within the reaction mixture prior to thermal cycling (ΔR at cycle 0) is comparable to the typical response observed for the DNA ladder (50–500 bp) at 1 ng/μL (Fig. 4). Mostly, electrical readouts are representative of the accumulated products, suggesting that nanopipettes or nanofluidic diodes with their surfaces regenerated through layer-by-layer assembly of cationic polyelectrolytes are capable of tracking the progress of PCR.

Real-time PCR is powerful as it provides a quantitative analysis for a specific sequence of DNA when present at even fewer than five copies (Klein, 2002). For a quantitative analysis, the exponential phase of the amplification curve is crucial wherein lies the *threshold cycle*, the number of cycles at which the signal intensity exceeds the background fluorescence, and needs to be carefully determined for the sample and the standards. To use nanopipettes for such analysis, a few improvements are in order. First, the background interference from the non-target species, although it could be subtracted out, has to be minimized for accurate evaluation of the threshold cycle. This would call for a more effective tip wash upon sample exposure. Due to the delicate tip structure, glass nanopipettes cannot withstand a stringent wash step, however. To better support the tip during an effective wash, nanopipettes could be centered in larger capillaries (Chu et al., 2007). Second, the signal strength from amplicons has to be further
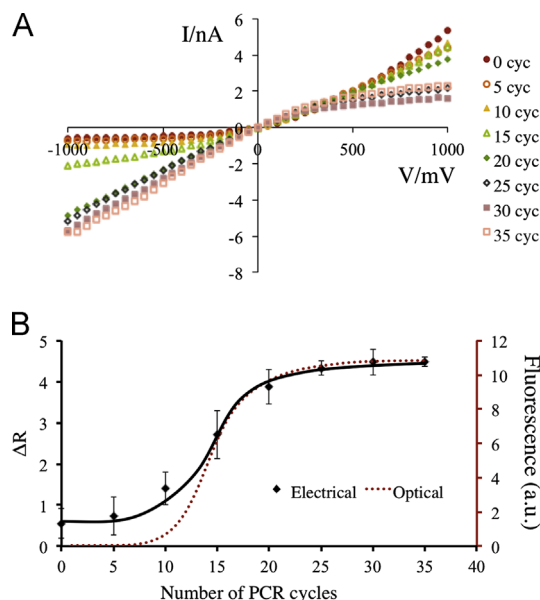
Fig. 6. Biosensor calibration for the quantitative PCR analysis. (A) A set of I–V curves all obtained from a single representative nanopipette upon the tip exposed to an unpurified PCR mixture terminated at a particular cycle (the legend). The mixtures were presented to the tip sequentially in no specific order and with each subsequent to a PLL cycle of tip surface regeneration. (B) Amplification plot derived from the measured I–V curves based on the absolute value of the shift in rectification ratio specific to the termination cycle of the PCR mixture. The symbols and error bars refer to the mean and ±1 standard deviation of the measurements from separate nanopipettes ($n = 5$). The dashed line (red) is the amplification plot and obtained from qPCR with the intercalating dye Sybr Green I. (For interpretation of the references to color in this figure legend, the reader is referred to the web version of this article.)

increased. The tip opening size has a direct impact on the ionic rectification and thus the signal strength. A smaller opening would lead to an enhanced field-effect from the adsorbed products. However, a lower limit on the practical tip size (~20 nm) would be expected considering that the nanoconfinement-induced structural reorganization of polyelectrolyte assemblies on the conical nanopores leads to surface charge degradation with the increased layers (Ali et al., 2010c). Nanopipettes with a smaller tip (below 80 nm) could be prepared from quartz capillaries using a laser-based puller. Alternatively, one could refer to the lithographically made nanofluidic diodes for a more controllable structure (Hlushkou et al., 2012). Such diodes are also more robust, amenable to microfluidic integration, and hence could benefit from a more effective sample delivery and wash through microfluidics.

It should be noted that the method presented here, as in the approach based on intercalating dyes, lacks the additional specificity offered by hybridization reporter probes. Hence, the diode will indiscriminately detect amplified products or products abundant in the starting sample. This requires extra caution when preparing samples to avoid false positives. We believe that the method, once refined, could be viable alternative to real-time PCR based on intercalating dyes and further integrated into downstream of a sample preparation module. The instrumentation, unlike the requirement of properly aligned bulky readout optics, may leverage a simple compact circuitry for $I-V$ measurements although a commercial patch clamp amplifier has been used here out of convenience. Further experiments targeting purified samples are needed to show the robustness of the method for a point-of-care setting.

4. Conclusions

Label-free real-time monitoring of the PCR progress through direct electrical readouts at sequential intervals is highly appealing from a standpoint of performing nucleic acid tests on integrated miniaturized devices at a point-of-care setting. Although the concept has been demonstrated here on simple glass nanopipettes, one could expect a comparable or better outcome with ionic rectifiers fabricated through lithography-based techniques for further scaling and integration. Equally intriguing is the notion of realizing field-effect sensing in a fluidic channel by modulating ionic convection rather than electronic conduction through a semiconductor device. The former is particularly favorable for the configuration of surface functionalization here through layer-by-layer assembly of polyelectrolytes. A new layer of nucleic acids electrostatically associated on the surface directly faces the channel and as such the influence of their intrinsic charge is more readily felt within the channel than would be experienced by a semiconductor device buried under a multitude of polyelectrolyte layers. Further, a simple fluidic-based solution to the field-effect sensing of amplicons suits upstream microfluidic processes for the extraction and amplification of nucleic acids. Future work is focused on scaling the concept to an integrated microsystem for real-time electrical PCR.

Acknowledgments

References

Abad, E., Juarros, A., Retolaza, A., Merino, S., Marie, R., Kristensen, A., 2011. Microelectronic Engineering 88 (3), 300–304.
Ali, M., Mafe, S., Ramirez, P., Neumann, R., Ensinger, W., 2009. Langmuir 25 (20), 11993–11997.
Ali, M., Neumann, R., Ensinger, W., 2010a. ACS Nano 4 (12), 7267–7274.
Ali, M., Schiedt, B., Neumann, R., Ensinger, W., 2010b. Macromolecular Bioscience 10 (1), 28–32.
Ali, M., Yameen, B., Cervera, J., Ramirez, P., Neumann, R., Ensinger, W., Knoll, W., Azzaroni, O., 2010c. Journal of the American Chemical Society 132 (24), 8338–8348.
Cheng, L.J., Guo, L.J., 2007. Nano Letters 7 (10), 3165–3171.
Cheng, L.J., Guo, L.J., 2010a. Microfluidics and Nanofluidics 9 (6), 1033–1039.
Cheng, L.J., Guo, L.J., 2010b. Chemical Society Reviews 39 (3), 923–938.
Chu, L.Y., Utada, A.S., Shah, R.K., Kim, J.W., Weitz, D.A., 2007. Angewandte Chemie International Edition 46 (47), 8970–8974.
Decher, G., 1997. Science 277 (5330), 1232–1237.
Eijkel, J.C.T., van den Berg, A., 2005. Microfluidics and Nanofluidics 1 (3), 249–267.
Fan, C.H., Plaxco, K.W., Heeger, A.J., 2003. Proceedings of the National Academy of Sciences United States of America 100 (16), 9134–9137.
Fritz, J., Cooper, E.B., Gaudet, S., Sorger, P.K., Manalis, S.R., 2002. Proceedings of the National Academy of Sciences United States of America 99 (22), 14142–14146.
Fu, Y.Q., Tokuhisa, H., Baker, L.A., 2009. Chemical Communications 32, 4877–4879.
Han, J., Craighead, H.G., 2000. Science 288 (5468), 1026–1029.
Heid, C.A., Stevens, J., Livak, K.J., Williams, P.M., 1996. Genome Research 6 (10), 986–994.
Hlushkou, D., Perry, J.M., Jacobson, S.C., Tallarek, U., 2012. Analytical Chemistry 84 (1), 267–274.
Hou, C.S.J., Milovic, N., Godin, M., Russo, P.R., Chakrabarti, R., Manalis, S.R., 2006. Analytical Chemistry 78 (8), 2526–2531.
Howorka, S., Siwy, Z., 2009. Chemical Society Reviews 38 (8), 2360–2384.
Kalman, E.B., Vlassiouk, I., Siwy, Z.S., 2008. Advaced Materials 20 (2), 293–297.
Karhanek, M., Kemp, J.T., Pourmand, N., Davis, R.W., Webb, C.D., 2005. Nano Letters 5 (2), 403–407.
Karnik, R., Castelino, K., Majumdar, A., 2006. Applied Physics Letters 88 (12), 123114–123116.
Karnik, R., Duan, C.H., Castelino, K., Daiguji, H., Majumdar, A., 2007. Nano Letters 7 (3), 547–551.
Kim, Y., Kim, K.S., Kounovsky, K.L., Chang, R., Jung, G.Y., dePablo, J.J., Jo, K., Schwartz, D.C., 2011. Lab on a Chip 11 (10), 1721–1729.
Klein, D., 2002. Trends in Molecular Medicine 8 (6), 257–260.
Kovarik, M.L., Zhou, K.M., Jacobson, S.C., 2009. Journal of Physical Chemistry B 113 (49), 15960–15966.
Luo, X.T., Hsing, I.M., 2009. Analyst 134 (10), 1957–1964.
Nam, S.W., Rooks, M.J., Kim, K.B., Rossnagel, S.M., 2009. Nano Letters 9 (5), 2044–2048.
Nam, S.W., Lee, M.H., Lee, S.H., Lee, D.J., Rossnagel, S.M., Kim, K.B., 2010. Nano Letters 10 (9), 3324–3329.
Nguyen, Q.H., Ali, M., Bayer, V., Neumann, R., Ensinger, W., 2010. Nanotechnology 21 (36), 365701–365708.
Piruska, A., Gong, M., Sweedler, J.V., Bohn, P.W., 2010. Chemical Society Reviews 39 (3), 1060–1072.
Plecis, A., Schoch, R.B., Renaud, P., 2005. Nano Letters 5 (6), 1147–1155.
Sa, N.Y., Fu, Y.Q., Baker, L.A., 2010. Analytical Chemistry 82 (24), 9963–9966.
Schoch, R.B., Han, J.Y., Renaud, P., 2008. Reviews of Modern Physics 80 (3), 839–883.
Siwy, Z., Heins, E., Harrell, C.C., Kohli, P., Martin, C.R., 2004. Journal of the American Chemical Society 126 (35), 10850–10851.
Siwy, Z.S., 2006. Advanced Functional Materials 16 (6), 735–746.
Tegenfeldt, J.O., Prinz, C., Cao, H., Chou, S., Reisner, W.W., Riehn, R., Wang, Y.M., Cox, E.C., Sturm, J.C., Silberzan, P., Austin, R.H., 2004. Proceedings of the National Academy of Sciences United States of America 101 (30), 10979–10983.
Umehara, S., Pourmand, N., Webb, C.D., Davis, R.W., Yasuda, K., Karhanek, M., 2006. Nano Letters 6 (11), 2486–2492.
Umehara, S., Karhanek, M., Davis, R.W., Pourmand, N., 2009. Proceedings of the National Academy of Sciences United States of America 106 (12), 4611–4616.
Vlassiouk, I., Smirnov, S., Siwy, Z., 2008. ACS Nano 2 (8), 1589–1602.
Vlassiouk, I., Kozel, T.R., Siwy, Z.S., 2009. Journal of the American Chemical Society 131 (23), 8211–8220.
Wei, C., Bard, A.J., Feldberg, S.W., 1997. Analytical Chemistry 69 (22), 4627–4633.
Zangle, T.A., Mani, A., Santiago, J.G., 2010. Chemical Society Reviews 39 (3), 1014–1035.
Zhang, J., Senger, B., Vautier, D., Picart, C., Schaaf, P., Voegel, J.C., Lavalle, P., 2005. Biomaterials 26 (16), 3353–3361.